Engineering Structures 112 (2016) 215–232

Contents lists available at ScienceDirect

Engineering Structures

journal homepage: www.elsevier.com/locate/engstruct

Experimental assessment of unreinforced exterior beam–column joints with deformed bars

Maria Teresa De Risi, Paolo Ricci *, Gerardo M. Verderame, Gaetano Manfredi

Department of Structures for Engineering and Architecture, University of Naples Federico II, Naples, Italy

ARTICLE INFO

Article history:
Received 16 May 2015
Revised 19 November 2015
Accepted 11 January 2016
Available online 29 January 2016

Keywords:
Exterior unreinforced RC joints
Non-conforming buildings
Cyclic test
Joint shear strength
Joint shear strain
Failure modes

ABSTRACT

In the performance assessment of typical existing buildings, seismic collapse safety might be significantly affected by non-linear behavior of joints that are involved in the failure mechanism, especially if they are characterized by poor structural detailing such as the lack of an adequate transverse reinforcement in the joint panel.

Unfortunately, commonly accepted tools to assess existing joints capacity are not available. Few reliable approaches for modeling all sources of nonlinearity are proposed in literature for poorly designed beam–column joints because of relatively poor information from experimental tests.

The present study aims at improving the understanding of seismic performance of exterior joints without transverse reinforcement in existing RC buildings through experimental tests.

Two full-scale exterior unreinforced beam–column joint sub-assemblages are tested under cyclic loading. The specimens are reinforced with deformed bars but they are different for beam longitudinal reinforcement ratio. Two different kinds of joint failure are expected, with or without the yielding of the adjacent beam. Strain gauges located on beam bars and displacement transducers on the joint panel allow the complete definition of both the main deformability contributions, namely fixed-end-rotation and shear strain of joint panel, highlighting the differences between failure modes.

Design criteria, adopted setup and experimental results are described and discussed. Finally, experimental results are compared with proposals from literature in terms of shear strength.

1. Introduction

Reinforced Concrete (RC) buildings designed for gravity loads only or according to obsolete seismic codes are widespread in Italian and Mediterranean building stock. For these buildings, beam–column joints represent a critical issue; the lack of capacity design principles leads to a low shear strength of the joint, potentially leading to a shear failure that limits the deformation capacity of adjoining beams and/or columns [1,2].

Past earthquakes showed that shear failure in beam–column joints can lead to building collapse [3], which often can be attributed to inadequate joint confinement. In recent earthquakes (e.g., Izmit 1999 [4], Tehuacan 1999 [5], Chi-Chi 1999 [6]), the inadequacy of building joints designed according to older standards was one of the main causes of severe damage or collapses. In particular, the observation of damage after L'Aquila earthquake (2009) indicated that RC buildings designed in Italy before the mid-1990s may have serious structural deficiencies especially in joint regions, mainly due to a lack of capacity design approach and/or poor detailing of reinforcement [7].

A significant amount of experimental research about seismic performance of RC beam–column joints has been carried out in the last forty years. The majority of the research literature has emphasized the improvement of the performance of RC beam–column joints through new design concepts and improved details, such as joint hoops or improved anchorage. Only in last years, an increasing interest about the analysis of unreinforced beam–column joints developed. In particular, experimental research is focused above all on exterior unreinforced joints [8], mainly due to the higher seismic vulnerability of this joint typology with respect to interior joints [9]. Two main goals are pursued in these experimental studies: (i) to assess seismic performance of unreinforced beam–column joints in "as-built" condition (for instance [10–13]); (ii) to evaluate the effectiveness of possible retrofitting strategies, such as the adoption of fiber-reinforced polymer materials [14–16], RC or steel jacketing [17–19], or post-installed anchors [20].

* Corresponding author.
E-mail addresses: mariateresa.derisi@unina.it (M.T. De Risi), paolo.ricci@unina.it (P. Ricci), verderam@unina.it (G.M. Verderame), gamanfre@unina.it (G. Manfredi).

http://dx.doi.org/10.1016/j.engstruct.2016.01.016
0141-0296/

In literature [21–24], comprehensive experimental databases of unreinforced exterior RC joints have been presented and discussed. In most of these tests, researchers focused their attention on joint shear strength and on the influence of several key parameters on this strength. In particular, generally investigated parameters are geometric parameters (for instance, the joint aspect ratio) or mechanical parameters (such as axial load ratio, concrete compressive strength, and longitudinal reinforcement ratio). Vice-versa, the number of experimental studies focused on (i) the main deformability sources due to joint, (ii) their contribution to the overall deformability, or (iii) local shear response of the joint panel is quite smaller. Nevertheless, a complete characterization of all the deformability contributions due to joints is paramount to understand the role of beam–column joints, not only in terms of strength, on nonlinear response of RC frames. Furthermore, a complete evaluation of joint local response allows properly modeling these elements into structural models for analysis of non-conforming RC frames.

This study aims at improving the understanding of seismic performance of unreinforced exterior joints in existing RC buildings, investigating on the influence of longitudinal reinforcement ratio on the joint shear strength, on one hand, and on the deformability contributions ascribable to the joint region on the response of the sub-assemblages, on the other hand. Two experimental tests on unreinforced exterior joints, without transverse beam, are tested under cyclic loading. The joint specimens are designed according to code prescriptions and design practices in force in Italy between 1970s and 1990s. Two distinct failure modes are expected: a joint shear failure prior to beam yielding (hereinafter referred to as J failure mode) and a joint shear failure following beam yielding (hereinafter referred to as BJ failure mode). The global experimental response and the evolution of observed damage are presented. The main deformation mechanisms of the RC joint region are discussed, and their contribution to the overall deformability is investigated. Moreover, local shear stress–strain response of joint panel is evaluated. Finally, main joint shear strength models existing in literature or codes are compared with experimental results.

The tests presented herein can provide a useful contribution to enhance the quite poor experimental database of unreinforced exterior joints, with respect to the corresponding database of reinforced exterior joints [8], and to better investigate about local response, not always analyzed in tests from literature.

2. Experimental program and setup

2.1. Specimens description

Two full-scale exterior unreinforced beam–column joint sub-assemblages (Fig. 1) have been tested under cyclic loading. The two tests are identical for geometry. Beam rectangular sectional area is 50 cm high (h_b = 50 cm) and 30 cm depth (b_b = 30 cm). Columns (top and bottom) have a square sectional area with height (h_c) equal to 30 cm. Column length was designed to be representative of typical interstorey height (3.40 m), and column shear length (L_c) is equal to 1.45 m. The beam length (up to the centerline of the column) is equal to 1.80 m, and its shear length is L_b = 1.65 m.

As shown in Fig. 1, in Test #1 the beam is symmetrically reinforced with 4 ϕ 20 bars for both reinforcement layers (corresponding to compression and tension reinforcement ratios equal to $\rho' = \rho = 0.84\%$); also the column is symmetrically reinforced with 4 ϕ 20 bars in top and bottom layers, corresponding to a total reinforcement ratio ($\rho' + \rho$) equal to 2.79%.

In Test #2, the beam is symmetrically reinforced with 4 ϕ 12 bars (corresponding to compression and tension reinforcement ratios equal to $\rho' = \rho = 0.30\%$); also the column is symmetrically reinforced with 4 ϕ 12 bars, corresponding to a total reinforcement ratio ($\rho' + \rho$) equal to 1.01%.

In both cases, ends of top and bottom beam longitudinal bars are bent at 90° into the joint core for a length of 20 cm. The transverse reinforcement consists of 8 mm diameter closed stirrups with both ends bent at 90° and 10 cm long. The stirrups are spaced at 10 cm along the beam and the column except within 62 cm of beam and column end, where the spacing is reduced to 5 cm to give adequate strength at the location where forces are applied during the test. The longitudinal reinforcement in the column extends continuously up through the joint from the bottom to the top of the column. The test unit reinforcement cages were constructed as shown in Fig. 1 and cast in place horizontally (see Fig. 2). A high-frequency vibrator was used to consolidate the concrete. Each test unit was allowed to cure for at least 72 h before they were removed from the forms.

2.2. Materials

Concrete compressive strength for all specimens was evaluated on four 15 × 15 × 15 cm^3 cubic samples (CSs) of the casted concrete. Values of 28-day cylindrical strength for each CS and their mean value are reported in Table 1. Commercial typology of the adopted reinforcing steel is B450C, i.e., class C reinforcement with f_{yk} = 450 MPa according to Annex C provisions of Eurocode 2 (EN 1992-1-1:2004 – Annex C) [25]. Steel typology B450C shows mechanical properties that can be assimilated to FeB44k typology, widespread in Italy between 1970s and 1990s. Tensile tests were carried out on three samples for each bar diameter. Table 2 reports mean values of their mechanical properties, namely yield strength (f_y), ultimate strength (f_t) and hardening ratio (f_t/f_y).

2.3. Design of specimens

Geometry and longitudinal reinforcement in beam and columns are defined by means of a simulated design procedure [26] of a perimeter 4-storey 5-bay frame according to code prescriptions and design practices in force in Italy between 1970s and 1990s. In particular, the analyzed specimens are intended to be representative of exterior joints of the first floor of such a frame. The specimen named Test #1 is related to a frame designed according to seismic prescriptions (for high seismicity level), in compliance with the Italian codes [27–29]. The specimen named Test #2 is related to a frame designed for gravity loads only.

Beam longitudinal reinforcement ($A_{s,b}$) is defined on the basis of flexural demand obtained from the simulated design, assuming an allowable stress for steel equal to 220 MPa (corresponding to a steel typology named FeB38k or FeB44k, commonly adopted in Italy in 70s–90s). Minimum amount of longitudinal reinforcement required in columns is slightly modified with respect to the simulated design and a weak beam–strong column hierarchy is obtained. Column axial load corresponding to gravity loads only is equal to 260 kN.

Transverse reinforcement in beam and columns was designed to avoid shear failure, in order to not preclude joint shear failure; whereas no transverse reinforcement was located in the joint panel zone, in compliance with code prescriptions in force in the reference time assumed for design.

Based on the adopted design practice and material mechanical properties, two failure modes are expected: a joint shear failure prior to beam yielding, for Test #1, and a joint shear failure following beam yielding, for Test #2.

According to ASCE/SEI 41 [9] a joint shear strength ($V_{jh,max}$) equal to 241.5 kN has been calculated, corresponding to a joint shear stress (τ_j) equal to 2.68 MPa. On the other hand, joint shear

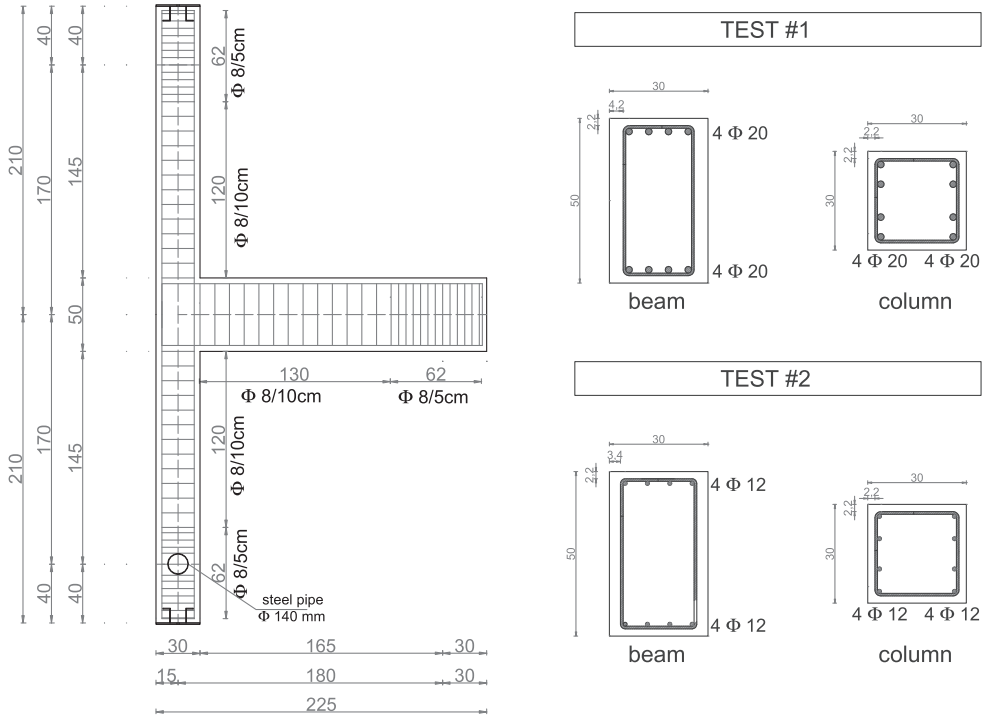

Fig. 1. Geometry and reinforcement details.

Fig. 2. Construction of specimens.

Table 1
Properties of concrete.

Cubic sample	Cylindrical compressive strength (f_c) (MPa)
CS1	27.2
CS2	29.2
CS3	31.2
CS4	27.4
Mean	28.8

Table 2
Properties of steel.

Diameter (mm)	Yield strength (f_y) (MPa)	Ultimate strength (f_t) (MPa)	Hardening ratio (f_t/f_y) (–)
20	487	596	1.22
12	459	560	1.22
8	492	607	1.23

demand at beam yielding ($V_{jh,yield}$) is calculated, on the basis of equilibrium equation, as

$$V_{jh,yield} = A_{s,b} f_y - A_{s,b} f_y \cdot (0.9d) \cdot [1 + h_c/(2L_b)]/(2L_c + h_b)$$

where d is the beam effective depth.

In particular, $V_{jh,yield}$ is equal to 530.4 kN ($>V_{jh,max}$) for Test #1, and 179.7 kN ($<V_{jh,max}$) for Test #2. Joint shear stresses corresponding to $V_{jh,max}$ are equal to 5.87 MPa and 2.00 MPa, respectively.

2.4. Test setup

A schematic of the loading apparatus is shown in Fig. 3(a). The column was mounted horizontally with pinned supports at both ends and the specimen was constrained to the strong floor by means of two rigid steel frames. Steel spherical hinges were placed between the beam end and the floor to avoid friction and to allow tip beam free movement. The axial load (N) was applied in load control using a small hydraulic jack and transferred to the column through four pre-stressed rods connected to strong steel plates located on the top and bottom of the column. In particular, a constant value of axial load equal to $N = 260$ kN (corresponding to an axial load ratio equal to $v = 0.10$) was applied.

A hydraulic actuator applied the lateral load in displacement control at the end of the beam by means of a loading collar. A load cell between the hydraulic actuator and the loading collar measured the quasi-static cyclic load applied to the beam. The actuator was pinned at the end to allow rotation during the test.

Twelve Linear Potentiometer sensors (LPs) adopted to measure joint shear strain and fixed-end-rotations were located in the joint panel along longitudinal reinforcement layers of beam and column and along the diagonals of the joint panels, as shown in Fig. 3(b). A wire potentiometer was placed at the end of the beam to measure beam deflection.

Strains in beam longitudinal reinforcement were measured, too, by means of six strain gauges (sgs) located as shown in Fig. 3(c) (three on a bar in the top layer and three on a bar in the bottom layer). Two additional Linear Variable Displacement Transducers (LVDTs) located along beam depth were used in Test #2 in order to have a more reliable measure of beam fixed-end-rotation contribution. Fig. 4 shows a photo of test setup (a) and joint panel zone (b).

2.5. Load pattern

Before beginning each test, the axial load was slowly applied to the column until the appropriate level was achieved. Then, the lateral load was applied cyclically, in a quasi-static way, at the end of the beam. The loading procedure consisted of displacement-controlled steps beginning at a 0.25% drift followed by steps of 0.50%, 0.75%, 1.00%, 1.50%, 2.00%, 3.00%, 4.00% and 6.00% drift. Each drift step consisted of 3 cycles of push and pull.

The term *drift* (D) represents the ratio between the imposed displacement and beam length (from the loaded end to the column centerline), namely, *drift* is equal to $\Delta_b/(L_b + h_c/2)$ and corresponds to the story drift [30].

The convention on signs adopted herein for drift and beam load (V_b), and the related local response (joint shear strain, γ_{joint}, rotation at the beam/joint interface, $\theta_{s,b}$, and rotation at the column/joint interface, $\theta_{s,c}$ – analyzed later in Section 4) is reported in Fig. 5.

3. Experimental results

In this section, lateral load–displacement response of tested specimens is analyzed, and the evolution of observed damage with increasing imposed displacement is described.

3.1. Global response

3.1.1. Test #1

The results in terms of beam lateral load versus drift response related to Test #1 are reported in Fig. 6(a), where experimental response appears quite symmetric during the push–pull cycles. The initial uncracked stiffness is equal to 15.0 kN/mm. Such a stiffness slightly decreased up to 12.7 kN/mm in the first millimeter of displacement applied to the beam end, and showed a more significant reduction when the applied drift ranged between 0.50% and 0.75%, when first joint panel cracking occurred.

Peak load was reached for a drift equal to 1.40% for positive loading direction and −1.38% for negative loading direction. Peak values of beam lateral load were 74.0 kN and −72.4 kN, respectively for positive and negative loading direction. Since beam yielding (evaluated through a section analysis) was expected to occur for a beam lateral load value of 155.6 kN, such a test can be classified as J-failure, i.e., joint shear failure occurring before yielding of the beam. Such a classification was confirmed by the measures of bar strains provided by the strain gauges.

The post-peak phase, controlled by joint failure, is characterized by a gradual degradation with a softening stiffness (calculated on the envelope of first cycles) equal to about −4% of the initial uncracked stiffness.

When the test was interrupted (first cycle at 6.00% drift), the strength reduction was equal to 47% and 53% of the peak load, in positive and negative direction, respectively, as reported in Fig. 6(c).

3.1.2. Test #2

The results in terms of beam lateral load versus drift response related to Test #2 are reported in Fig. 6(b). Also in this case, experimental response appears quite symmetric during the push–pull cycles. Test #2 exhibited an initial uncracked stiffness equal to 15.1 kN/mm. Such a stiffness decreased up to 14.5 kN/mm in the first millimeter of displacement applied to the beam end, and showed a more significant reduction when the applied drift ranged between 0.25% and 0.50%, when first cracks along beam–joint interface started to occur (associated with a localized strength reduction).

Peak load was reached for a drift equal to 0.88% for positive loading direction and −0.69% for negative loading direction. Peak values of beam lateral load were 58.3 kN and −54.0 kN, respectively for positive and negative loading direction. Since beam yielding (evaluated through a section analysis) was expected to occur

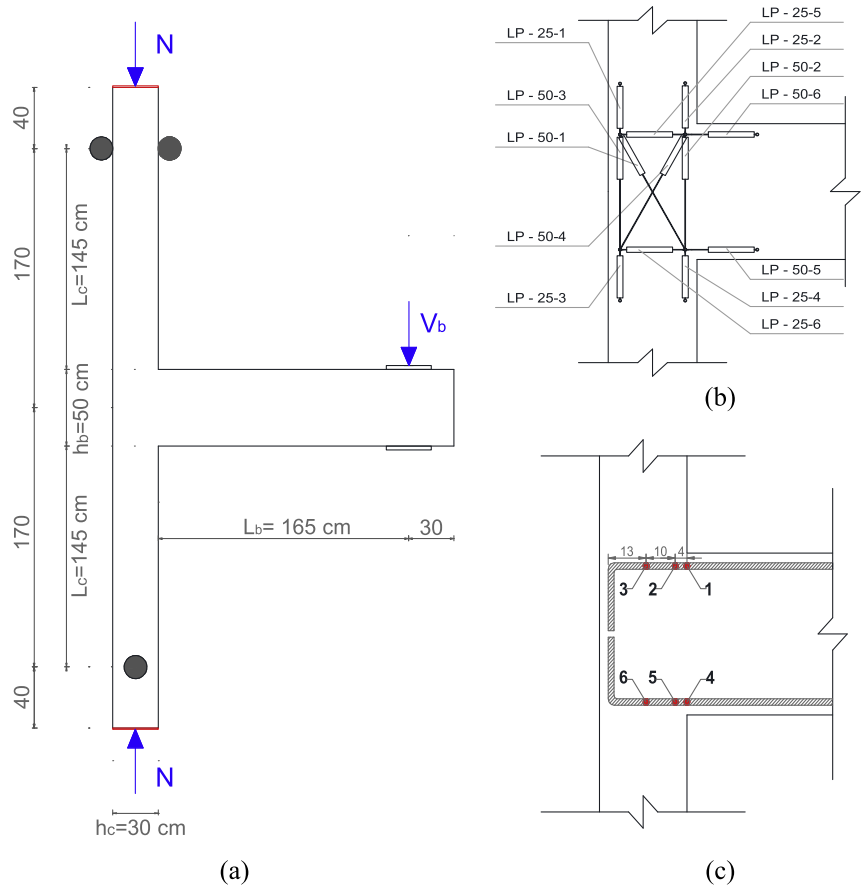

Fig. 3. Test setup (a), joint panel instrumentation (b) and strain gauges location (c).

Fig. 4. Test setup (a) and joint panel instrumentation (b).

for a beam lateral load value of 52.9 kN, such a test can be classified as BJ-failure, i.e., joint shear failure occurring after yielding of beam. The yielding of beam section was confirmed by the measures of bar strains provided by the employed strain gauges. At the same time, the peak load is lower than beam flexural strength (65.5 kN), for both loading directions, confirming that peak strength is limited by the achievement of joint shear failure.

The post-peak phase, controlled by joint failure, is characterized by a gradual degradation with a softening stiffness (calculated on the envelope of first cycles) equal to about −6% of the initial uncracked stiffness.

Test #2 was interrupted when the third cycle at 2.00% drift was fully completed, because a sudden elongation of the hydraulic jack occurred, as it will be better explained later (Section 3.3). When the test was interrupted (third cycle at 2.00% drift), the strength reduction was equal to 49% and 56% with respect to the peak load, respectively in positive and negative directions, as reported in Fig. 6(d). The strength reduction, evaluated at the first cycle at

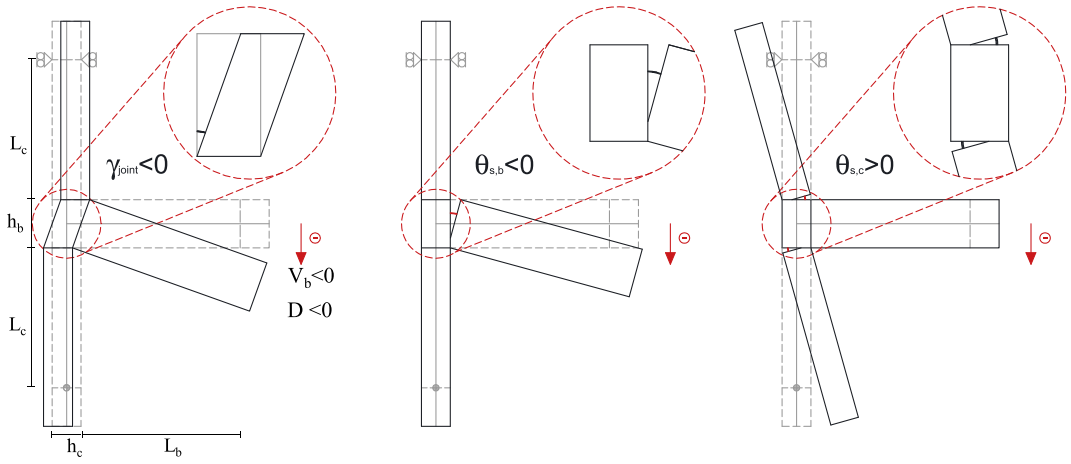

Fig. 5. Convention on signs.

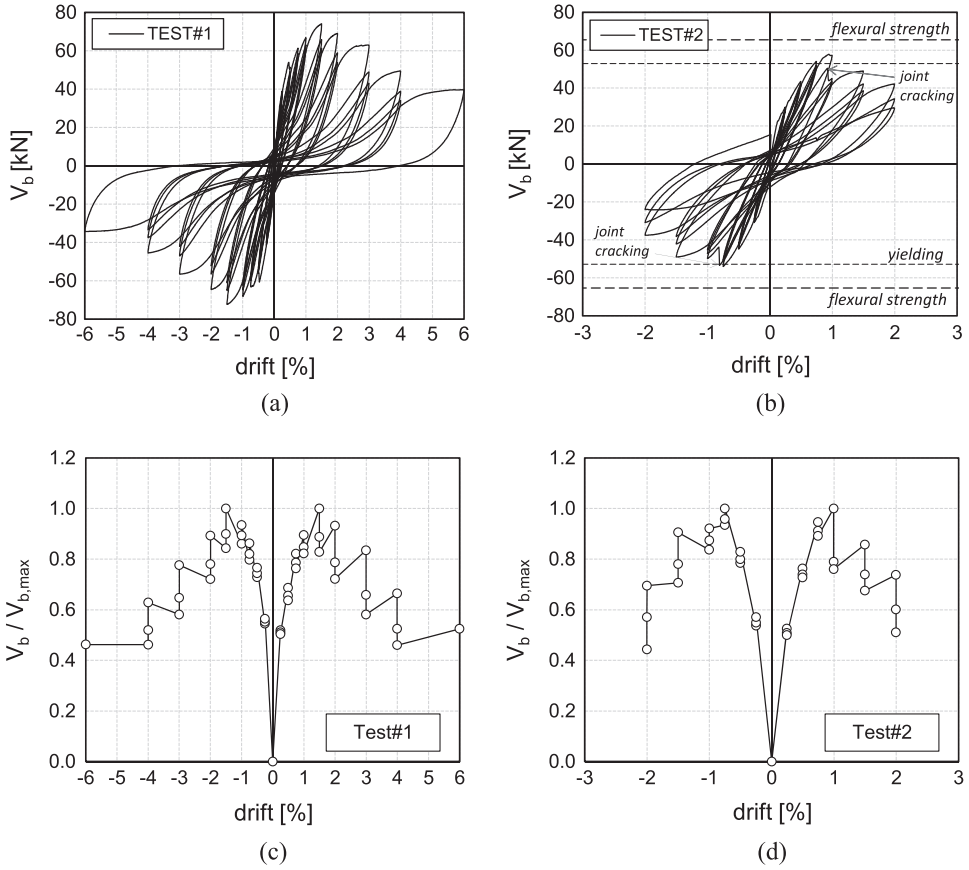

Fig. 6. Beam lateral load versus drift: cyclic response of Test #1 (a), cyclic response of Test #2 (b), envelope of Test #1 (c), envelope of Test #2 (d).

Table 3
"Peak points" and yielding beam load.

	$V^{+}_{b,max}$ (kN)	D^{+}_{peak} (%)	$V^{-}_{b,max}$ (kN)	D^{-}_{peak} (%)	$V_{b,y}$ (kN)	Failure mode
Test #1	74.0	1.40	−72.4	−1.38	155.6	J
Test #2	58.3	0.88	−54.0	−0.69	52.9	BJ

2.00% drift, was equal to 26% and 31% of the peak load, respectively in positive and negative directions.

Peak values of beam lateral load for positive ($V^{+}_{b,\max}$) and negative ($V^{-}_{b,\max}$) loading directions and corresponding drifts are summarized in Table 3, together with beam load values corresponding to beam yielding ($V_{b,y}$). Finally, the ultimate drift, defined as the drift at 20% drop in strength respect to the peak lateral load (evaluated on the envelope of the first cycles), is equal to 3.00% for Test #1 and 1.80% for Test #2 (see Figs. 6(c) and 6(d)).

3.2. Observed damage

3.2.1. Test #1

Hairline cracks at beam–joint interface appeared at first loading stages, namely already for 0.25% drift corresponding to a beam load equal to 37 kN (predicted value for beam cracking was equal to 28 kN). First diagonal cracks in the joint panel started to appear when a drift ratio equal to 0.50% was imposed, starting from corner B (see Fig. 7), first in negative loading direction, at −60 kN beam load, and then in positive direction, for a beam load value of +54 kN. Between 0.50% and 0.75% drift, diagonal cracks in the joint panel occurred and spread along column longitudinal bars. At 3.00% drift, existing cracks in the joint panel increased their width and concrete cover spalling started to occur from corner C (see Fig. 7). Concrete cover spalling was complete when a drift value of 6.00% was reached.

In Fig. 7 the evolution of joint panel damage state is visually reported and a more severe cracking pattern can be observed along the diagonal A–D. Fig. 8 shows the final damage state of the specimen. (i) the significant damage of joint panel, (ii) the spalling of concrete cover away from the lateral side of joint; (iii) no buckling of column longitudinal reinforcement in the joint region, and (iv) a limited crack width at beam–joint interface can be noted. Table 4 summarizes the evolution of the observed damage for Test #1 described above.

Furthermore, in Fig. 9 the envelope (of the first cycles) of displacement (δ_{LP}) measured by means of the LPs located along the diagonals of the joint panel is reported versus the applied drift level, for Test #1; elongation is taken as positive. Data are cut at 2.00% drift, when cracks significantly involved the support points of LPs, causing unreliable measurements. LP 50-4 provides the higher values of displacement (δ_{LP}) (up to about 7 mm at 2.00% drift), consistent with the more significant cracking pattern of joint panel along the diagonal A–D observed before (Fig. 7).

3.2.2. Test #2

Also in this case, first hairline cracks at beam–joint interface appeared at early loading stage, namely already for 0.25% drift corresponding to a beam load equal to 29 kN (quite close to the predicted value for beam cracking, i.e., 23 kN). Slightly wider cracks started to appear at beam–joint interface when a drift ratio equal to 0.50% was imposed, as shown in Fig. 10.

When the drift value was equal to 1.00%, diagonal cracks in the joint panel occurred and spread along column longitudinal bars, first in negative loading direction, at −54 kN beam load, and then in positive direction, for a beam load value of +49 kN. At 1.50% drift, cracks at beam–joint interface increased progressively their width, mainly due to fixed-end-rotation of the beam, and new diagonal cracks appeared in the joint core. At 2.00% drift, existing cracks significantly increased their width and buckling of longitudinal bars of column and sudden complete cover spalling occurred at the third cycle. In Fig. 10 the evolution of joint panel damage state is visually reported, and a more severe cracking pattern can be observed along the diagonal B–C.

Fig. 11 shows the final damage state of the specimen. (i) a severe damage level of the lateral side of joint caused by concrete cover spalling; (ii) the sudden buckling of column longitudinal reinforcement in the joint region, (iii) the quite moderate damage level in the joint panel, and (iv) a more important crack width at beam–joint interface with respect to Test #1 can be noted. Table 5 summarizes the evolution of the observed damage for Test #2.

Moreover, in Fig. 12 the envelope (of the first cycles) of displacement δ_{LP} versus drift is reported for Test #2. Data are cut at the second sub-cycle at 2.00% drift, since, at the third cycle, the cracks significantly involved the support points of LPs, causing unreliable measurements. In this case, LP 50-1 provides the higher values of displacement (δ_{LP}) (up to about 6 mm at 2.00% drift), consistent with the more significant cracking pattern of joint panel along the diagonal B–C observed before (Fig. 10).

3.2.3. Damage states

Several measures of the deterioration of RC members due to earthquake loading have been presented in literature in last decades. Most of these indices express the damage level to individual elements and are generally based on observed damage or displacement ductility ratio and hysteretic dissipated energy. Specifically for unreinforced beam–column joints in older RC frames similar to test specimens presented herein, Pagni and Lowes [31] identify thirteen Damage States (DSs) – from DS0 to DS12 – that characterize the progression of damage under earthquake loading. These DSs were defined on the basis of data obtained from laboratory test specimens as well as guidelines for post-earthquake repair and interviews with professionals, in order to best characterize the progression of damage in joints and best determine the appropriate method of repair for the component. Herein such DSs are used to describe the damage sustained by each specimen under cyclic loading (as in [18]).

As suggested by Pagni and Lowes [31], DS at each applied drift level is defined on the basis of: cracking pattern, peak shear strength, yielding of beam longitudinal reinforcement (if any), cracks opening (where possible), concrete spalling, and buckling of column longitudinal reinforcement (if any). In particular, the more severe DS that can be recognized at each drift level is plotted in Fig. 13 for both tests.

It can be noted that Test #1 shows a gradual increase in damage level, starting from hairline cracks at beam–joint interface (DS0) and cracks in the joint core (from DS1 to DS3) up to cracks extension in columns (DS9) and, finally, a quite distributed crushing of concrete in the joint core (DS11) and cover. Note that DS7 corresponds to the achievement of the peak strength and the beginning of joint shear strength degradation (as it will be shown also in Section 4).

Vice-versa, in Test #2 the evolution of damage is faster, from DS0 to buckling of column longitudinal reinforcement (DS12). In this case, first joint cracking (DS1–DS3) and beam longitudinal reinforcement yielding (DS4) occur at the same drift level than DS7.

Fig. 13 clearly shows that, at a given drift level, DS is higher for Test #2 than for Test #1, confirming the faster damage evolution for Test #2.

3.3. Final condition of Test #2

As observed previously, Test #2 was interrupted when the third cycle at 2.00% drift was reached; in fact, at this step, a sudden elongation of the hydraulic jack acting on column occurred, as shown in Fig. 14(a), together with joint concrete cover spalling and sudden buckling of column longitudinal bars. In Fig. 14(b) experimental displacement measured by LVDT-D (located versus the vertical face of the joint), is reported depending on the beam lateral load, and the initial step of the sudden elongation of the hydraulic jack is indicated by a red[1] circle.

[1] For interpretation of color in Fig. 14, the reader is referred to the web version of this article.

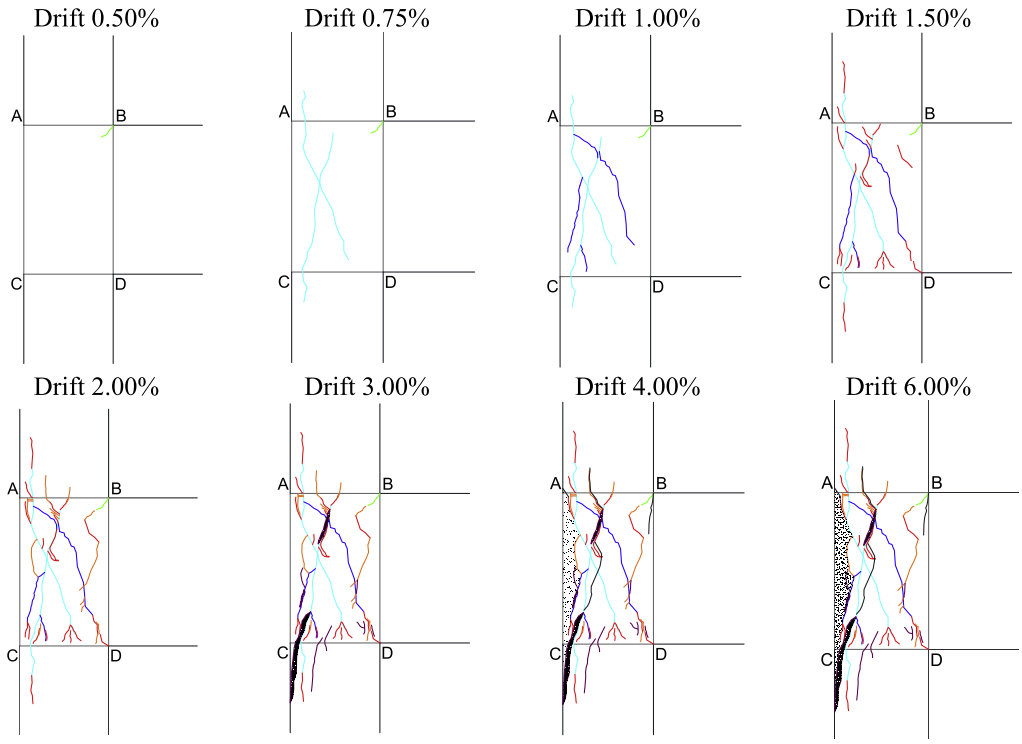

Fig. 7. Evolution of damage – Test #1.

Fig. 8. Final damage state: joint panel and beam–joint interface – Test #1.

Table 4
Description of the evolution of damage during Test #1.

Cycle	Drift (%)	Damage description		
		Joint	Beam	Column
1	0.25	No damage	Hairline cracks at beam–joint interface along beam width	No damage
2	0.50	First light cracks at corner B	Crack opening at beam–joint interface along beam width	–
3	0.75	Diagonal cracks in the joint panel spreading along column longitudinal bars	–	–
4	1.00	New diagonal cracks and spreading of existing cracks	–	–
5	1.50	New diagonal cracks	–	–
6	2.00	New diagonal cracks	–	Spreading of cracks along longitudinal bars
7	3.00	Spreading of existing cracks and beginning of concrete cover spalling starting from corner C	–	–
8	4.00	New diagonal cracks, significant cracks lengthening, concrete cover spalling along A–C side	–	–
9	6.00	Complete concrete cover spalling	–	–

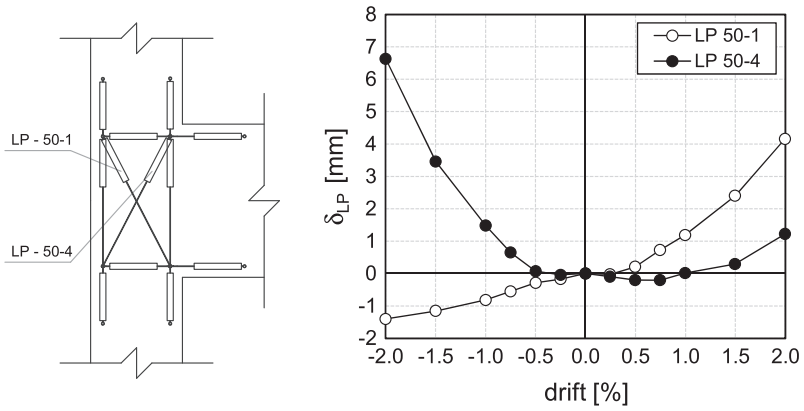

Fig. 9. LPs displacements along the diagonals of the joint panel – Test #1.

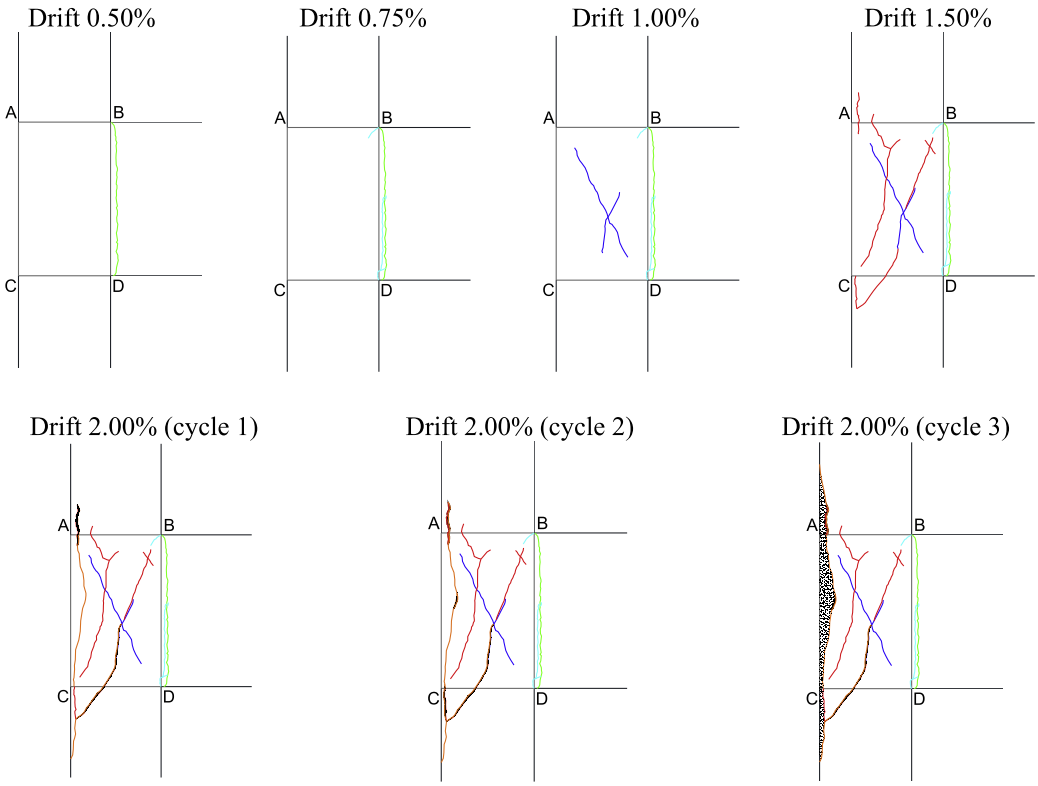

Fig. 10. Evolution of damage – Test #2.

Fig. 11. Final damage state: joint panel and beam–joint interface – Test #2.

Table 5
Description of the evolution of damage during Test #2.

Cycle	Drift (%)	Damage description		
		Joint	Beam	Column
1	0.25	No damage	Hairline cracks at beam–joint interface	No damage
2	0.50	–	Light cracks at beam–joint interface	–
3	0.75	–	New cracks at beam–joint interface	–
4	1.00	Light diagonal cracks in the joint panel	–	–
5	1.50	New diagonal cracks in the joint panel and light cracks along column longitudinal bars	Lengthening of existing cracks at beam–joint interface	Cracks along longitudinal bars
6-1	2.00	New diagonal cracks in the joint panel	–	–
6-2		Significant lengthening of existing cracks	–	–
6-3		Concrete cover spalling along A–C side	–	Bar buckling

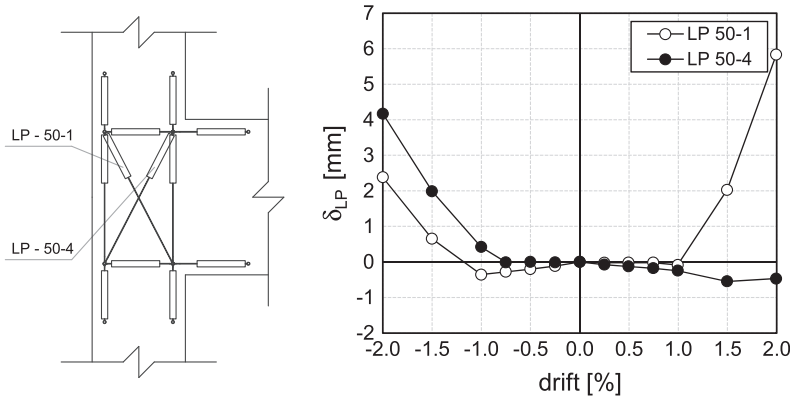

Fig. 12. LPs displacements along the diagonals of the joint panel – Test #2.

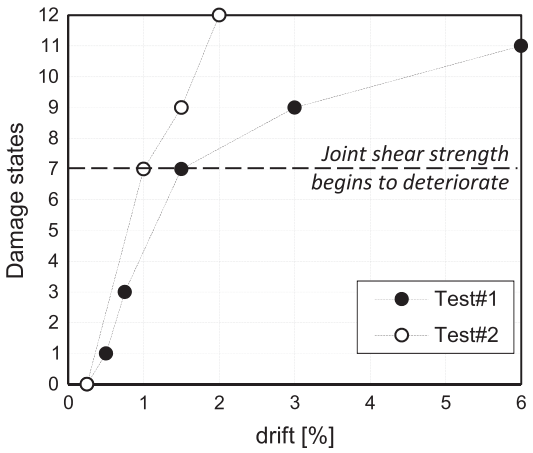

Fig. 13. DSs according to Pagni and Lowes [31].

It can be asserted that the sudden elongation of the hydraulic jack is most likely due to the sudden reduction in axial stiffness of "column + joint" system, caused by joint concrete cover spalling and buckling of column longitudinal bars. This outcome is also confirmed by the evidence that no sudden increase in the elongation of the hydraulic jack was observed in Test #1 (see Fig. 14(a)), since cover spalling occurred more gradually (see Table 4) and, above all, no buckling of column longitudinal reinforcement occurred, thanks to the higher bar diameter with respect to Test #2 (20 mm versus 12 mm).

The sudden elongation of the hydraulic jack, which caused the interruption of the test prematurely respect to the established loading pattern, could appear to depict the "beginning" of an axial load failure for this test. Therefore, this aspect is investigated and discussed in this section by post-processing of the experimental data.

In literature, tests that exhibited this kind of failure are in a very limited number. Furthermore, different approaches were used to define the onset of joint axial failure [32], for instance, the drop in column axial load, or a joint axial shortening beyond a certain threshold, or the full disintegration of the joint. In the present study, since column axial load was constant during the test, the second criterion should be applied to identify a potential joint axial load failure. Unfortunately, such a criterion cannot be applied in this case, due to the reduced reliability of measures from LPs since the second sub-cycle at 2% drift.

In Hassan [32] a database has been collected with experimental tests of ten unreinforced joints characterized by an axial load failure, identified according to one of the criteria previously listed. According to Hassan [32] and Hassan and Moehle [33], the axial capacity of column longitudinal bars in the joint region (due to buckling or sway collapse) should be always achieved after a sliding mechanism along the diagonal shear failure plane, caused by the shear damage sustained by the joint panel. Hassan and Moehle's thesis was based on the observation of axial failure modes for RC joints in the collected database and it was similar to the proposal related to shear damaged RC columns by Elwood and Moehle [34].

Nevertheless, the final damage state of joint panel in Test #2 is not characterized by a main diagonal shear crack that identifies a diagonal shear failure surface (because of the quite moderate final damage state of the joint panel). Moreover, Test #2 has a peculiarity with respect to tests analyzed by Hassan [32]. In fact, column bars buckling occurred before (and not after) a (potential) diagonal sliding in the joint core. This condition has most likely been promoted by the higher slenderness of column longitudinal reinforcement (with respect to tests analyzed by Hassan and Moehle [33]),

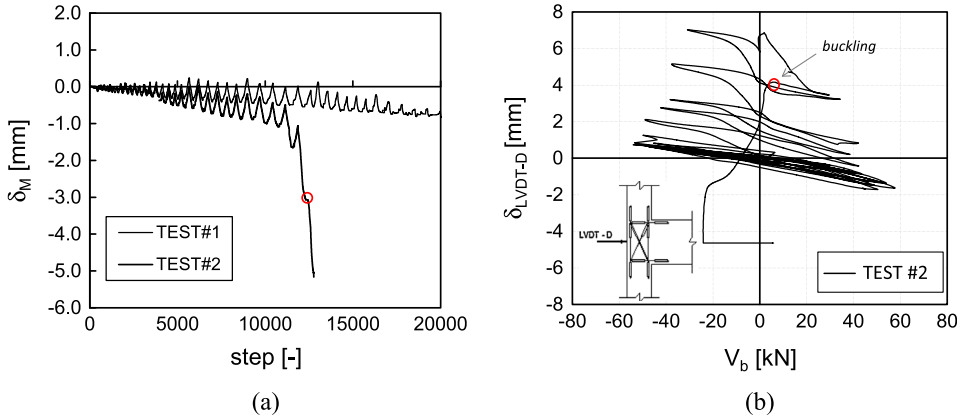

Fig. 14. Bar buckling: LVDT-D displacement versus beam lateral load V_b (a), hydraulic jack acting on column (b).

characterized by a bar diameter equal to only 12 mm. Much higher diameters characterize tests in Hassan and Moehle's database.

In conclusion, the sudden elongation of the hydraulic jack at the end of Test #2 (at 2.00% drift) cannot be considered, by itself, an evidence of joint axial load failure. This conclusion is also confirmed by two more issues, as shown in Fig. 15. In particular, Figs. 15(a) and 15(b) show a visual comparison between the final damage states related to Test #5 in Pantelides et al.'s experimental campaign [11] and Test #2 presented herein, respectively. It can be noted that Test #5, which is one of the few (four) exterior joints in Hassan's database [32], shows a high damage level due to shear demand in the joint core when axial load failure occurred, differently from the final damage state observed in Test #2. Secondary, in Fig. 15(c) the empirical relationship between axial load ratio and maximum drift reached prior to the axial failure proposed by Hassan and Moehle [33] is shown: it can be observed that Test #2 belongs to the "axial failure safe zone", and, therefore, according to such a relationship, the final condition of Test #2 cannot be classified as axial load failure.

4. Local behavior

In this section, most significant local measurement data, related to main deformation mechanisms observed in specimens, are discussed.

4.1. Joint panel response

Linear potentiometers located on the joint panel are employed to calculate joint shear strain, as suggested and adopted by previous experimental works (e.g., [35,32,24,36]), according to which joint shear strain can be expressed as shown in Eq. (1):

$$\gamma_{\text{joint},i} = \frac{\varepsilon_\theta - \varepsilon_x \cos^2\theta - \varepsilon_y \sin^2\theta}{\sin\theta\cos\theta} \tag{1}$$

where $\gamma_{\text{joint},i}$ is the joint shear strain obtained using a certain set of strain measures, ε_x and ε_z are strains in the horizontal and vertical directions, respectively, and ε_θ is the strain in the diagonal direction at an angle θ from the horizontal axis. Four estimates of the joint shear strain are obtained by four triangles of LPs located in the joint panel (see Fig. 3(b)) by using Eq. (1). Joint strain (γ_{joint}) is finally calculated as the mean of these four estimates. Sign convention for shear strain is related to beam displacement sign convention: negative joint shear strain corresponds to downward beam displacement (see Fig. 5).

Joint shear stress is calculated based on equilibrium equations. In particular, joint shear demand V_{jh} is calculated according to Eq. (2):

$$V_{\text{jh}} = T - V_c \tag{2}$$

where T is the tensile force acting in beam longitudinal bars and V_c represents column shear force. Tensile force T is calculated according to Eq. (3):

$$T = \frac{M_b}{d^*} = \frac{V_b \cdot L_b}{(\beta \cdot d)} \tag{3}$$

where L_b is the beam clear length and d^* the internal lever arm of beam section, evaluated as $d^* = (\beta \cdot d)$, where d is the effective depth. The coefficient β is calculated through the equivalence between the "exact" beam yielding moment, calculated by means

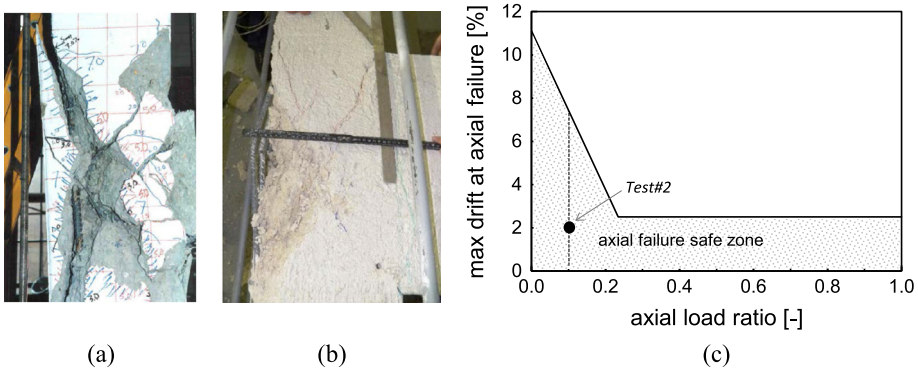

Fig. 15. Final damage states of Test #5 by Pantelides et al. [11] (a), and of Test #2 (b); empirical relationship for axial load failure detection by Hassan and Moehle [33].

of a section analysis, and the "simplified" beam yielding moment, calculated through a constant internal level arm as $M_{b,y} = A_s f_y(\beta \cdot d)$, similarly to other literature studies [22,23]. As a result, β is equal to 0.90.

Column shear force V_c is calculated from equilibrium equations, as shown in Eq. (4):

$$V_c = \frac{V_b \cdot (L_b + h_c/2)}{(2L_c + h_b)} \tag{4}$$

where $(L_b + h_c/2)$ is the total length of the beam, and $(2L_c + h_b)$ is the total length of bottom and top columns (see also Fig. 5 for notation). Joint shear stress (τ_j) can be calculated as the ratio between joint shear force (V_{jh}) and joint horizontal area (A_{jh}). Hereinafter, $\tau_j/\sqrt{f_c}$ will represent joint shear stress divided by the square root of concrete compressive strength f_c.

In Fig. 16(a) and (b), experimental responses in terms of $\tau_j/\sqrt{f_c}$ versus γ_{joint} are reported for Test #1 and Test #2, respectively. The corresponding envelopes (related to the first cycles) are reported in Fig. 16(c), whereas in Fig. 16(d) the same envelopes are shown in terms of principle tensile stress, $p_t/\sqrt{f_c}$, versus γ_{joint}.

Data are represented until LPs measures are considered reliable, i.e., until cracks significantly involved the support points of LPs, namely until the end of the third sub-cycle at 2.00% drift, for Test #1, and of the second sub-cycle at 2.00% drift, for Test #2.

4.1.1. Test #1

In Test #1, the joint shear stress–shear strain response is significantly asymmetric, with higher deformability in negative loading direction: at the end of the first sub-cycle at 2.00% drift, γ_{joint} in negative loading direction is equal to about three times the corresponding joint strain in positive loading direction. The peak values of $\tau_{j,max}/\sqrt{f_c}$ are 0.53 and −0.52 $(MPa)^{0.5}$ for positive and negative direction, respectively. The corresponding γ_{joint} are equal to 0.53% and −1.18%, respectively. The $p_t/\sqrt{f_c}$ versus γ_{joint} response is asymmetric also in terms of strength, due to the variation of axial load acting on joint caused by shear force transferred by the beam. The peak values of $p_{t,max}/\sqrt{f_c}$ are 0.37 and −0.28 $(MPa)^{0.5}$ for positive and negative direction, respectively.

4.1.2. Test #2

Also for the Test #2, the joint shear stress–shear strain response is significantly asymmetric, with higher deformability in positive loading direction. The peak values of $\tau_{j,max}/\sqrt{f_c}$ are 0.41 and −0.38 $(MPa)^{0.5}$ for positive and negative direction, respectively; the corresponding γ_{joint} are equal to 0.04% and −0.07%, respectively. Negative peak point is substantially coincident with joint cracking ($\tau_{j,cr}/\sqrt{f_c} = -0.38(MPa)^{0.5}$), since they were reached at the end of the elastic phase of behavior of the joint. When positive peak point was reached, joint cracking occurred, causing a significant reduction in stiffness and strength, followed by a strength recovery up to 0.32 $(MPa)^{0.5}$ for positive direction at 0.64% of γ_{joint}.

Also in this case, the $p_t/\sqrt{f_c}$ versus γ_{joint} response is asymmetric also in terms of strength. The peak values of $p_{t,max}/\sqrt{f_c}$ are 0.25 and −0.18 $(MPa)^{0.5}$ for positive and negative direction, respectively.

Table 6 shows the values of $\tau_j/\sqrt{f_c}$ corresponding to first shear cracking and peak strength of the joint panel. In particular, the onset of first cracks in joint panel is evaluated taking into account both the evolution of joint damage (see Table 4 and Table 5) and the variation of stiffness in global ($V_{beam} - D$) response when first joint cracks appeared.

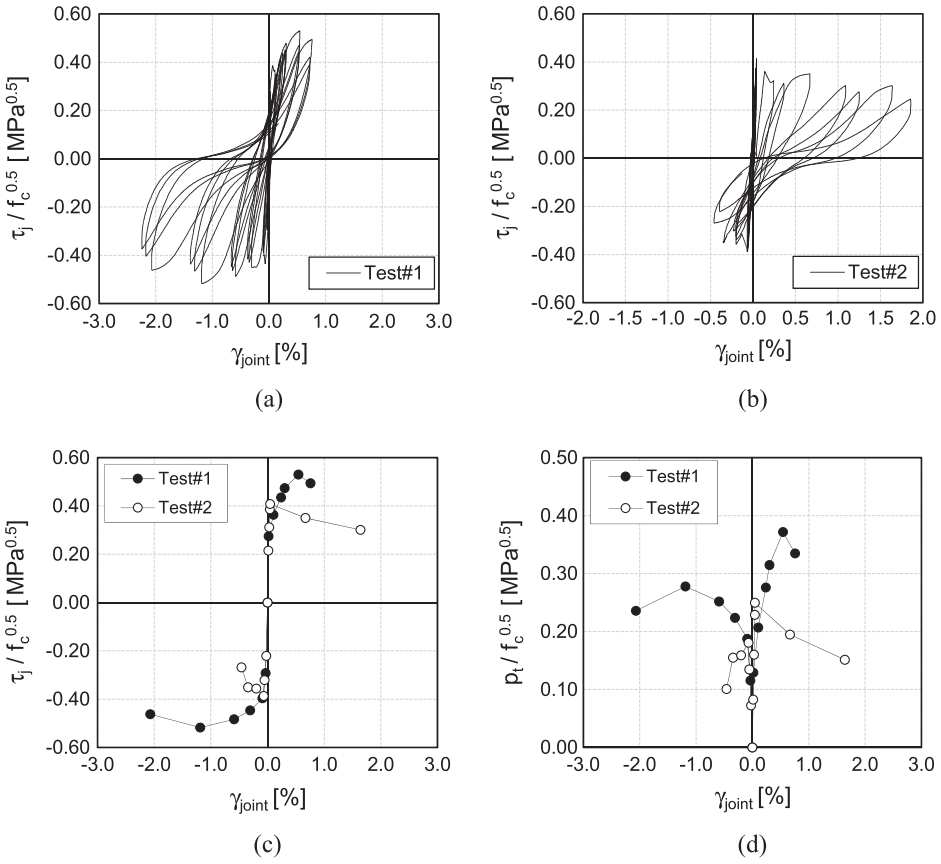

Fig. 16. Joint panel response: shear stress $\tau_j/\sqrt{f_c}$ – shear strain γ_j relationship for Test #1(a), and for Test #2 (b); envelope of experimental response in terms of shear stress $\tau_j/\sqrt{f_c}$ – strain γ_{joint} (c), envelope of experimental response in terms of principle tensile $p_t/\sqrt{f_c}$ – strain γ_{joint} (d).

Table 6
Experimental values of $\tau_j/\sqrt{f_c}$ corresponding to shear cracking and peak strength of joint panel.

	$V_{b,cr}$ (kN)	$V_{b,max}$ (kN)	L_b (mm)	$L_b - h_c/2$ (mm)	$2L_c$ (mm)	$\tau_{j,cr}/\sqrt{f_c}$ ($\sqrt{MPa}$)	$\tau_{j,max}/\sqrt{f_c}$ ($\sqrt{MPa}$)	$\tau_{j,y}/\sqrt{f_c}$	$\tau_{j,flex}/\sqrt{f_c}$
Test #1	60.0	74.0	1800	1650	3400	0.43	0.53	1.11	–
Test #2	54.0	58.3	1800	1650	3400	0.38	0.41	0.38	0.46

Table 6 shows that Test #2 exhibited a lower joint shear strength $\tau_{j,max}/\sqrt{f_c}$ respect to Test #1. This outcome is ascribable to the evidence that joint shear strength cannot generally overcome the joint shear stress demand corresponding to beam flexural strength ($\tau_{j,flex}/\sqrt{f_c}$) – in weak beam–strong column cases. In fact, since the definition itself of joint shear V_{jh} (see Eqs. (2)–(4)), the (maximum) beam flexural strength corresponds to the maximum joint shear stress. Because of the lower beam longitudinal reinforcement ratio, Test #2 is characterized by a $\tau_{j,flex}/\sqrt{f_c}$ lower than the maximum joint shear strength $\tau_{j,max}/\sqrt{f_c}$ exhibited in Test #1. However, in Test #2, joint shear failure occurs after beam yielding and $\tau_{j,max}/\sqrt{f_c}$ does not reach the value $\tau_{j,flex}/\sqrt{f_c}$. This outcome also confirms proposals from literature [37] according to which the joint shear strength decreases with the ductility demand in beam increasing. Such a reduction prevents the achievement of the beam flexural strength.

In Fig. 17, γ_{joint} is reported as a function of the imposed drift level. The joint shear strain is evaluated at the end of the first cycle of each imposed drift value (see Fig. 16(c)), until joint shear strain can be reliably calculated.

In Test #1 the shear strain of the joint panel rapidly increases after joint cracking (drift = 0.50%). When the peak strength is attained (drift = 1.50%) the maximum γ_{joint} is equal to 1.19% and increases up to 2.07% in post-peak phase (at 2.00% drift). Again, the higher deformability under negative imposed displacements is observed.

In Test #2, too, the shear strain is not significant until joint cracking occurs. In post-cracking (or post-peak) phase, γ_{joint} increases rapidly up a maximum value of 1.64% (at 2.00% drift). In this case, a higher deformability under positive imposed displacements is observed, as previously described.

Summarizing, in the post-cracking phase of the joint panel, given a fixed drift level, higher values of γ_{joint} are observed in Test #1 (J-failure) compared with Test #2 (BJ-failure), as it will be better explained in Section 4.3.

4.2. Rotation at beam(column)/joint interface

The rotation at the beam(column)/joint interface – $\theta_{s,b}$ ($\theta_{s,c}$) – and, thereby, its contribution to the overall deformability – can be estimated through LPs located along longitudinal bars of column at the interface with joint panel (Fig. 18). In particular, since for Test #2 a more significant deformability contribution due to beam was expected, two more LVDTs (located on beam depth) were employed (only) for this test (see Fig. 18(b)), in order to have a more accurate measure of θ_s.

Starting from each pair of LPs or LVDTs (providing displacement measurements d_1 and d_2) located at a distance a, the rotation at the beam (column)/joint interface (θ_s) is calculated according to Eq. (5):

$$\theta_s = \frac{d_2 - d_1}{a} \tag{5}$$

Note that such a rotation does not correspond to "fixed-end rotation" since LPs provide the measure of the whole crack width at the interface, including the slippage of longitudinal bars both from the panel zone and from the element. Only the former contribution leads to fixed-end rotation, properly representing a source of deformability provided by the joint, whereas the latter leads to a rotation that should be considered as part of beam (column) deformability.

Figs. 19(a) and 19(b) show the rotation θ_s as a function of the imposed drift for Tests #1 and #2, respectively, evaluated for beam, top column and bottom column.

Experimental data are plotted until the support points of the corresponding LPs were affected by significant cracks (i.e., when a drift value equal to 2.00% was reached). As for γ_{joint} in Fig. 17, also θ_s is evaluated at the end of the first sub-cycle for each drift value. In both tests, it can be observed that θ_s is generally lower for the columns than for the beam.

4.3. Analysis of deformability contributions

In this section, the contributions due to joint, beam and columns to the overall deformability of the sub-assemblage are evaluated by analyzing the relationship between the quantities γ_{joint}, $\theta_{s,b}$ and $\theta_{s,c}$ (calculated at the end of the first sub-cycle for each imposed drift level, as previously) with the imposed drift. Beam top displacement (Δ_b) due to each of the analyzed quantities is calculated as shown in Eq. (6) (see also Fig. 5 for notation):

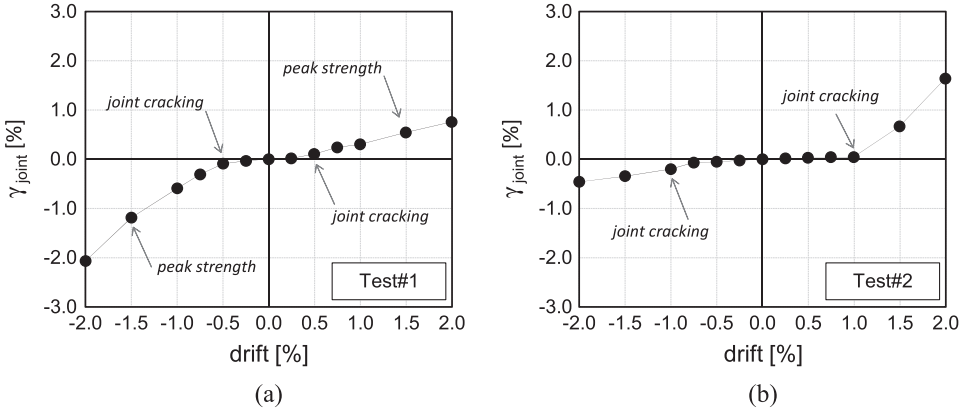

Fig. 17. γ_{joint} versus global imposed drift: Test #1 (a) and Test #2 (b).

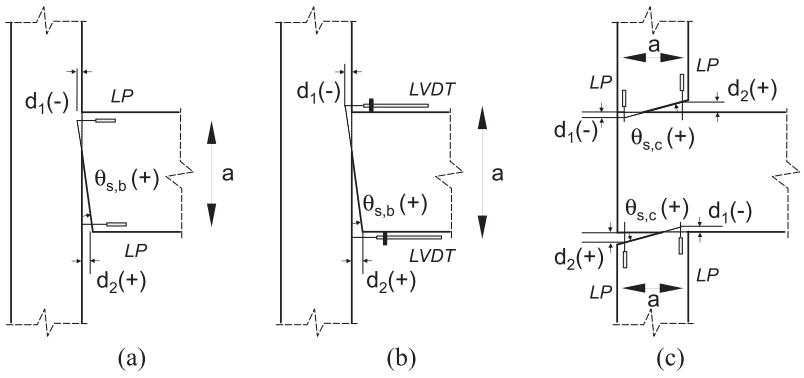

Fig. 18. Rotation at the beam/ (a and b) and column/ (c) joint interface.

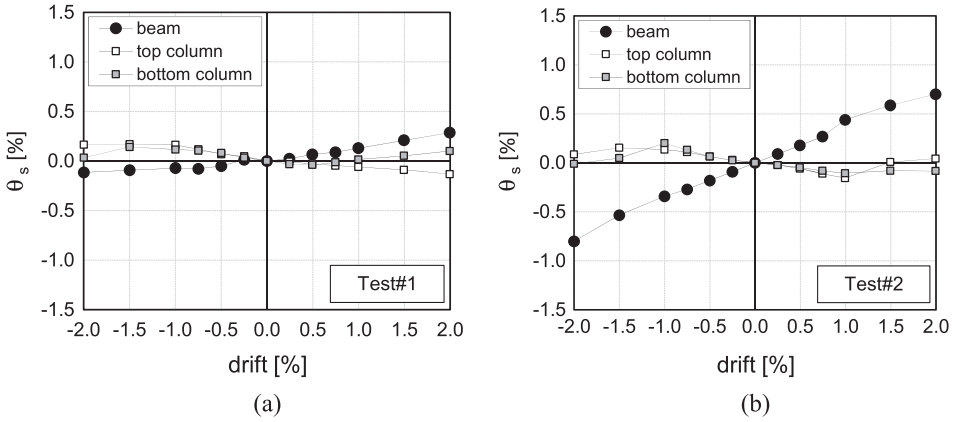

Fig. 19. Rotation θ_s related to beam, top column and bottom column: Test #1 (a) and Test #2 (b).

$$\Delta_b^{\gamma_{joint}} = \gamma_{joint} \cdot L_b - (\gamma_{joint} \cdot h_b)\frac{(L_b + 0.5h_c)}{(2L_c + h_b)}$$
$$\Delta_b^{\theta_{s,b}} = \theta_{s,b} \cdot L_b \qquad (6)$$
$$\Delta_b^{\theta_{s,c}} = (\theta_{s,c}^{top} + \theta_{s,c}^{bot}) \cdot L_c \cdot \frac{(L_b + 0.5h_c)}{(2L_c + h_b)}$$

where $\theta_{s,c}^{top}$ and $\theta_{s,c}^{bot}$ represent the rotation θ_s for top and bottom columns, respectively.

By dividing Δ_b due to γ_{joint}, $\theta_{s,b}$ and $\theta_{s,c}$ for the total imposed Δ_b, the percentage contribution to the global deformability is obtained for each component. Such contributions are shown in Fig. 20 as a function of the total imposed drift. For both tests, it can be observed that the sum of deformability percentage contributions due to joint shear strain and rotation at beam–joint interface, ($\theta_{joint} = \gamma_{joint} + \theta_{s,b}$), represents the majority of the imposed drift.

For Test #1 (Fig. 20(a)) – which exhibited a J-failure mode – θ_{joint} reaches a maximum of 70% of the imposed drift at the peak point

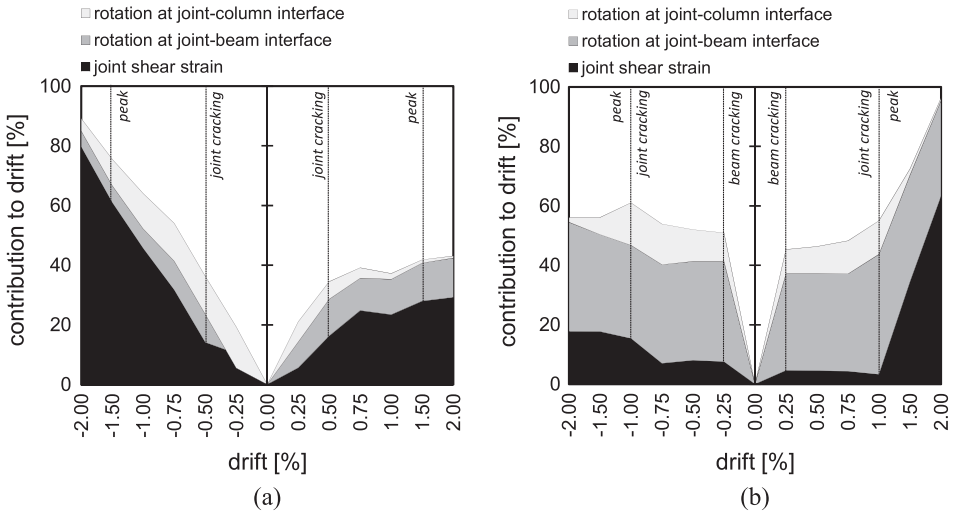

Fig. 20. Contributions to the overall imposed drift: Test #1 (a) and Test #2 (b).

(drift = 1.50%) and about the 80% at 2.00% drift (in negative loading direction). In particular, after the cracking of the joint panel (drift = 0.50%), the shear strain contribution due to γ_{joint} is systematically predominant with respect to the contribution due to rotation at the beam(column)/joint interface.

For Test #2 (Fig. 20(b)) – which exhibited a BJ-failure mode – θ_{joint} reaches a maximum value of about 95% at 2.00% drift (positive loading direction). The contribution due to rotation $\theta_{s,b}$ is the main contribution to θ_{joint} until cracking of the joint panel occurs. Vice-versa, after cracking of joint, the contribution of γ_{joint} rapidly increases, while $\theta_{s,b}$ is almost constant, despite yielding of longitudinal reinforcement.

Such trends are consistent with the expected deformation mechanisms, based on the observed failure modes. Finally, the contribution that misses to reach 100% in Fig. 20 is due to flexural deformability of beam and columns, and progressively reduces its weight for increasing drift levels.

4.4. Beam bars strains

In this section strain measures related to the beam longitudinal reinforcement bars are plotted for strain gauges located at beam–joint interface, namely sg #1 and sg #4.

Steel strain of longitudinal beam bars in Test #1, see Fig. 21(a), reaches a maximum value of 0.137% and thus it is always much lower than the strain corresponding to yielding ($\varepsilon_{s,y}$ = 0.243%), thus confirming the failure mode classification for this test as J-failure.

Steel strain of longitudinal beam bars in Test #2, see Fig. 21(b), reaches a maximum value of 0.288% (when 1% imposed drift was reached) and thus overcomes the yielding strain ($\varepsilon_{s,y}$ = 0.230%), thus confirming that Test #2 can be classified as BJ-failure.

5. Joint shear strength: comparison with literature models

Local joint panel responses of Tests #1 and #2 are compared with strength models existing in literature. Experimental shear stresses, corresponding to the shear cracking ($\tau_{j,cr}/\sqrt{f_c}$) and to the shear strength ($\tau_{j,max}/\sqrt{f_c}$) of the panel zone, are compared with the corresponding values predicted by some of the main formulations from codes and literature.

In particular, experimental values of $\tau_{j,cr}/\sqrt{f_c}$ are compared with predicted shear cracking stress provided by Uzumeri [38] and Priestley [39], as shown in Table 7. Uzumeri's formulation provides a shear cracking stress that is the closest to the experimental values for both tests: the ratio between experimental and predicted values is 1.10 and 0.97 for Test #1 and Test #2, respectively.

Similarly, experimental shear strength is compared with the main formulations proposed by codes [9] and literature [39,21,8].

ASCE/SEI 41 [9] provides a value of $\tau_{j,max}/\sqrt{f_c}$ that depends on joint typology and transverse reinforcement ratio; for exterior unreinforced joints without transverse beams, shear strength can be obtained from Eq. (7):

$$\tau_{j,max}/\sqrt{f_c} = 0.50 \tag{7}$$

Priestley [39] suggests limiting the maximum value of principal tensile stress to $0.42\sqrt{f_c}$, therefore:

$$\frac{p_{t,max}}{\sqrt{f_c}} = \frac{1}{2\sqrt{f_c}}\left(-\sigma + \sqrt{\sigma^2 + 4\tau^2}\right) = 0.42 \tag{8}$$

Park and Mosalam [21] propose a mechanical approach accounting for joint shear strength degradation after beam yielding and directly providing a definition of the failure mode:

$$\tau_{j,max}\Big/\sqrt{f_c} = k\left[\frac{\cos\theta}{\cos(\pi/4)}\right] \tag{9}$$

Table 7
Shear cracking stress: comparison between experimental and predicted values.

	Formulation	Test #1 ($\sqrt{MPa}$)	Test #2 ($\sqrt{MPa}$)
Experimental	–	0.43	0.38
Uzumeri [38]	$(\tau_{j,cr}/\sqrt{f_c}) = 0.29\sqrt{1 + 0.29\frac{N}{A_j}}$	0.39	0.39
Priestley (1992)	$(\tau_{j,cr}/\sqrt{f_c}) = 0.29\sqrt{1 + \frac{N}{0.29\sqrt{f_c}A_j}}$	0.49	0.49

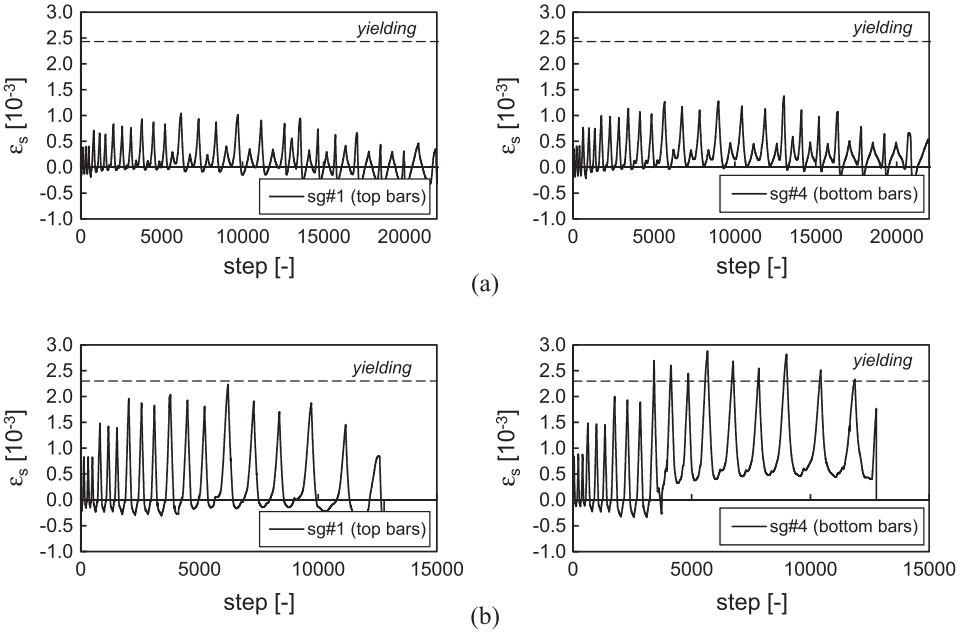

Fig. 21. Beam bars strain: Test #1 (a), Test #2 (b).

Table 8
Experimental joint shear strength and models from literature (values corresponding to lowest prediction errors are highlighted in bold).

Specimen	$\tau_{j,max}/\sqrt{f_c}$ (MPa$^{0.5}$)					$p_{t,max}/\sqrt{f_c}$ (MPa$^{0.5}$)	
	Exp.	ASCE/SEI 41 [9]	Park and Mosalam [21]	Jeon et al. [8] MARS	Jeon et al. [8] MLR	Exp.	Priestley [39]
Test #1	0.53	**0.50**	0.73	0.70	0.70	0.37	0.42
Error	–	−6%	+36%	+32%	+32%	–	+14%
Test #2	0.41	0.50 (0.46)	**0.40**	**0.42**	**0.42**	0.25	0.42 (0.30)
Error	–	+22% (+12%)	−2%	+2%	+2%	–	+68% (+20%)

where θ is a function of the joint aspect ratio (beam height/column depth) and "k" is a strength factor accounting for the effect of the beam longitudinal reinforcement ratio. When "k" is equal or higher than the unit, a J-failure occurs; the value of "k" is limited to 1.0. The minimum value of Eq. (9) is reached when "k" is equal to 0.4. When the parameter "k" ranges between 0.4 and 1.0 a BJ-failure occurs.

Based on an extended database of experimental tests [23], Jeon et al. [8] propose new probabilistic joint shear strength models. By using a set of candidate predictor variables (independent input variables), a conventional multiple linear regression method (MLR) and an advanced machine-learning method of multivariate adaptive regression splines (MARS) are adopted, in a log-transformed space, to search for significant predictor variables.

As a result, the joint shear strength obtained from the MARS method, for unreinforced joints, is obtained as in Eq. (10):

$$\begin{aligned}\ln(\tau_{j,max}) = {} & 1.73 - 4.19BF_1 - 1.43BF_2 + 1.37BF_3 - 0.71BF_4 \\ & + 0.38BF_5 + 0.26BF_6 + 4.67BF_7 + 0.57BF_8 \\ & + 0.78BF_9 - 0.25BF_{10} - 3.29BF_{11} - 1.97BF_{12} \\ & - 0.14BF_{13} - 3.45BF_{14} - 3.97BF_{15}\end{aligned} \quad (10)$$

where BF_i are parameters defined as functions of the normalized log-transformed independent variables ξ_j, which, in turn, depend on the following parameters: concrete compressive strength f_c; maximum joint shear demand τ_d; in-plane and out-of-plane geometry factors JP and TB; joint aspect ratio h_b/h_c; beam-to-column depth ratio; joint eccentric factor; column axial load factor; ratio of provided to required column depth to beam rebar; column-to-beam nominal moment strength ratio M_R; and the ratio of intermediate column reinforcement strength to design joint shear demand θ. The reader is referred to [8] for further details.

By adopting the same notation, the joint shear strength obtained from the MLR method, for unreinforced joints, is obtained as in Eq. (11):

$$\begin{aligned}\ln(\tau_{j,max}) = {} & -0.81 + 0.46\ln(f_c) + 0.50\ln(\tau_d) + 0.68\ln(JP) \\ & + 0.62\ln(TB) - 0.25\ln(h_b/h_c) + 0.08\ln(M_R) \\ & + 0.14\ln(\theta)\end{aligned} \quad (11)$$

A summary of joint shear strength from different models for Test #1 and Test #2 is reported in Table 8.

Note that models by ASCE/SEI 41 [9] and Priestley [39] do not consider the influence of beam longitudinal reinforcement on joint shear strength. When they are adopted, the joint shear strength calculated in compliance with models is successively limited to the maximum allowable joint shear stress (namely that corresponding to beam flexural capacity). This limiting value is shown in Table 8 within round brackets.

Vice-versa, models by Park and Mosalam [21] and Jeon et al. [8] explicitly consider the influence of beam longitudinal reinforcement on joint shear strength, by means of the parameters "k" or τ_d, respectively. In these cases, the joint shear strength is calculated in compliance with the model proposal without any limitation.

5.1. Test #1

The comparison reported in Table 8 shows that the code proposal adopted herein as a reference [9] slightly underestimates the experimental strength (with a percentage error of about 6%); however, this model provides the best predictive capacity. The other models provide higher overestimations of shear strength, from a minimum of 14% (model by Priestley [39]) to a maximum of 36% (model by Park and Mosalam [21]).

5.2. Test #2

In this case, the comparisons reported in Table 8 highlight a very good predictive capacity of models by Park and Mosalam [21] and Jeon et al. [8] (which show an absolute percentage error of 2%), namely the only models, among those considered herein, which explicitly consider the influence of beam longitudinal reinforcement on joint shear strength. Vice-versa, models by Priestley [39] and ASCE/SEI 41 [9] overestimate the experimental strength by 68% and 22%, respectively. This overestimation decreases up to 20% and 12%, respectively, when joint shear strength proposed by models is limited to the joint shear stress at the beam flexural strength demand, as previously explained.

6. Conclusions

In the present work, experimental results of two tests on unreinforced exterior RC beam–column joints were analyzed. The joint specimens were designed according to code prescriptions and design practices in force in Italy between 1970s and 1990s; in particular, the Test #1 specimen was designed according to seismic prescriptions, whereas the Test #2 specimen for gravity loads only. Depending on the different beam longitudinal reinforcement ratio of the two specimens, two distinct failure modes were expected, namely joint shear failure prior to beam yielding for Test #1, and joint shear failure following beam yielding for Test #2.

Experimental results, in terms of lateral load–displacement response, showed that:

- in Test #1, the attainment of maximum strength was controlled by joint failure, without flexural yielding of the beam;
- in Test #2, the attainment of maximum strength was controlled by joint failure and followed the flexural yielding of the beam; actually, peak load was higher than the expected load at flexural yielding and lower than the expected flexural strength of the beam.

Measures from strain gauges (located on beam longitudinal bars at beam–joint interface) confirmed the expected failure modes.

Test #1 showed a quite sever damage level due to shear demand in the joint core at the end of the test, together with a complete cover spalling from the side of the joint. Test #2 was

interrupted because of the sudden buckling of column longitudinal reinforcement passing through the joint panel, even if, in this case, a more moderate damage level due to shear demand was observed in the joint core at the end of test.

It was also highlighted that the higher the beam longitudinal reinforcement ratio, the higher the joint shear strength, confirming proposals from literature according to which joint shear strength decreases as ductility demand in beam increases.

The analysis of local responses highlighted that the sum of the main deformability contributions due to joints (joint panel shear strain and rotation at beam/joint interface) represented the major part of the imposed drift for both tests. In particular:

- in Test #1 (J-failure mode), after the cracking of the joint panel, the joint shear strain contribution was systematically predominant with respect to the contribution due to rotation at the beam(column)/joint interface;
- in Test #2 (BJ-failure mode), the rotation at beam/joint interface contribution was systematically predominant until cracking of the joint panel occurred; vice versa, after joint cracking, the contribution of joint shear strain rapidly increased, while the rotation at beam/joint interface was almost constant, despite yielding of longitudinal reinforcement.

Experimental shear stress, corresponding to the shear cracking of the panel zone and to shear strength, were compared with the corresponding values predicted by some of the main formulations proposed in codes and literature. Uzumeri's formulation for shear stress at cracking provides values that are the closest to the experimental values for both tests. As far as peak shear strength is concerned, surprisingly, model by code [9] shows, on average between the two tests, the best predictive capacity with respect to other empirical models.

The experimental tests described herein can provide a very useful contribution to the characterization of the experimental behavior of unreinforced RC beam–column joints, toward future studies related to the validation/proposal of nonlinear models for the assessment of existing non-ductile RC buildings, accurately modeling all the sources of deformability due to beam–column joints.

Acknowledgements

This work was developed under the financial support of STRESS S.c.a.r.l. STRIT Project "PON Ricerca e Competitività 2007-2013". This support is gratefully acknowledged.

References

[1] Park S, Mosalam KM. Simulation of reinforced concrete frames with nonductile beam-column joints. Earthq Spectra 2013;29(1):233–57.
[2] Celik OC, Ellingwood BR. Modeling beam-column joints in fragility assessment of gravity load designed reinforced concrete frames. J Earthq Eng 2008;12:357–81.
[3] Moehle JP, Mahin SA. Observations on the behavior of reinforced concrete buildings during earthquakes. In: Ghosh SK, editor. Earthquake-resistant concrete structures inelastic response and design SP-127. Detroit: American Concrete Institute; 1991.
[4] Sezen H, Elwood KJ, Whittaker AS, Mosalam KM, Wallace JW, Stanton JF. Structural engineering reconnaissance of the August 17, 1999 earthquake: Kocaeli (Izmit), Turkey. PEER-2000/09, Berkeley: Pacific Earthquake Engineering Research Center, University of California; December 2000.
[5] Earthquake Engineering Research Institute. EERI special earthquake report – September 1999. The Tehuacan, Mexico, Earthquake of June 15; 1999. <http://www.eeri.org/>.
[6] Earthquake Engineering Research Institute. EERI special earthquake report – December 1999. The Chi-Chi, Taiwan Earthquake of September 21; 1999. <http://www.eeri.org/>.
[7] Ricci P, De Luca F, Verderame GM. 6th April 2009 L'Aquila earthquake, Italy: reinforced concrete building performance. Bull Earthq Eng 2011;9(1):285–305.
[8] Jeon J-S, Shafieezadeh A, DesRoches R. Statistical models for shear strength of RC beam-column joints using machine-learning techniques. Earthq Eng Struct Dynam 2014;43(14):2075–95 [November 2014].
[9] ASCE/SEI 41. Seismic rehabilitation of existing buildings. Reston, VA, USA: American Society of Civil Engineers; 2007.
[10] Clyde C, Pantelides CP, Reaveley LD. Performance-based evaluation of exterior reinforced concrete buildings joints for seismic excitation. PEER report no. 2000/05. Berkeley, USA: Pacific Earthquake Engineering Research Center, University of California; 2000.
[11] Pantelides CP, Hansen J, Nadauld J, Reaveley LD. Assessment of reinforced concrete building exterior joints with substandard details. PEER report, no 2002/18. USA: Pacific Earthquake Engineering Research Center, University of California, Berkeley; 2002.
[12] Wong HF. Shear strength and seismic performance of non-seismically designed RC beam–column joints. PhD thesis. Hong Kong University of Science and Technology; 2005.
[13] Masi A, Santarsiero G, Nigro D. Cyclic tests on external RC beam-column joints: role of seismic design level and axial load value on the ultimate capacity. J Earthq Eng 2013;17.1:110–36.
[14] Tsonos AG, Papanikolaou KV. Post-earthquake repair and strengthening of reinforced concrete beam-column connections (theoretical & experimental investigation). Bull-NZ Soc Earthq Eng 2003;36(2):73–93.
[15] Antonopoulos CP, Triantafillou TC. Experimental investigation of FRP-strengthened RC beam-column joints. J Compos Constr 2003;7(1):39–49.
[16] Di Ludovico M, Balsamo A, Prota A, Verderame GM, Dolce M, Manfredi G. Preliminary results of an experimental investigation on RC beam-column joints. In: 6th International conference on FRP composites in civil engineering (CICE 2012), Rome, Italy, 13–15 June; 2012 [Paper 02-511].
[17] Karayannis CG, Chalioris CE, Sirkelis GM. Local retrofit of exterior RC beam-column joints using thin RC jackets – an experimental study. Earthq Eng Struct Dynam 2007;37:727–46.
[18] Karayannis CG, Sirkelis GM. Strengthening and rehabilitation of RC beam–column joints using carbon-FRP jacketing and epoxy resin injection. Earthq Eng Struct Dynam 2008;37(5):769–90.
[19] Santarsiero G, Masi A. Seismic performance of RC beam–column joints retrofitted with steel dissipation jackets. Eng Struct 2015;85:95–106.
[20] Genesio G. Seismic assessment of RC exterior beam-column joints and retrofit with haunches using post-installed anchors. PhD thesis. Germany: University of Stuttgart; 2012.
[21] Park S, Mosalam KM. Analytical model for predicting the shear strength of unreinforced exterior beam-column joints. ACI Struct J 2012;109:149–59.
[22] Park S, Mosalam KM. Parameters for shear strength prediction of exterior beam–column joints without transverse reinforcement. Eng Struct 2012;36:198–209.
[23] Jeon J-S. Aftershock vulnerability assessment of damaged reinforced concrete buildings in California. PhD thesis. GA: School of Civil and Environmental Engineering, Georgia Institute of Technology; 2013.
[24] De Risi MT. Seismic performance assessment of RC buildings accounting for structural and non-structural elements. PhD thesis. Naples, Italy: University of Naples Federico II; 2015.
[25] CEN. European standard EN1992-1-1. Eurocode 2: design of concrete structures – Part 1–1: general rules and rules for buildings. Brussels: Comité Européen de Normalisation; 2004.
[26] Verderame GM, Polese M, Mariniello C, Manfredi G. A simulated design procedure for the assessment of seismic capacity of existing reinforced concrete buildings. Adv Eng Softw 2010;41(2):323–35.
[27] Decreto Ministeriale n. 40 del 3/3/1975. Approvazione delle norme tecniche per le costruzioni in zone sismiche. G.U. n. 93 dell'8/4/1975; 1975 [in Italian].
[28] Decreto Ministeriale del 7/3/1981. Dichiarazione di zone sismiche nelle regioni Basilicata, Campania e Puglia; 1981 [in Italian].
[29] Decreto Ministeriale del 14/02/1992. Norme tecniche per il calcolo, l'esecuzione ed il collaudo delle strutture in cemento armato, normale e precompresso e per le strutture metalliche; 1992 [in Italian].
[30] Bonacci JF, Wight JK. Displacement-based assessment of reinforced concrete frames in earthquakes. ACI Special Publication 162; 1996.
[31] Pagni CA, Lowes LN. Fragility functions for older reinforced concrete beam-column joints. Earthq Spectra 2006;22(1):215–38.
[32] Hassan WM. Analytical and experimental assessment of seismic vulnerability of beam-column joints without transverse reinforcement in concrete buildings. PhD dissertation. California, USA: University of California, Berkeley; 2011.
[33] Hassan WM, Moehle J. Quantification of residual axial capacity of beam-column joints in existing concrete buildings under seismic load reversals. Compdyn 2013 – Kos Island, Greece, 12–14 June; 2013.
[34] Elwood KJ, Moehle JP. Axial capacity model for shear-damaged columns. ACI Struct J 2005;102(4):578–87.
[35] Engindeniz M. Repair and strengthening of pre-1970 reinforced concrete corner beam-column joints using CFRP composites. PhD thesis. Civil and Environmental Engineering Department, Georgia Institute of Technology; August 2008.

[36] Ricci P, De Risi MT, Verderame GM, Manfredi G. Experimental assessment of unreinforced exterior beam-column joints with plain bars. Eng Struct; 2016 (submitted for publication).
[37] Hakuto S, Park R, Tanaka H. Seismic load tests on interior and exterior beam–column joints with substandard reinforcing details. ACI Struct J 2000;97 (1):11–25.
[38] Uzumeri SM. Strength and ductility of cast-in-place beam-column joints. In: From the American concrete institute annual convention, symposium on reinforced concrete structures in seismic zones, San Francisco, 1974. No. SP-53; 1977.
[39] Priestley MJN. Displacement-based seismic assessment of reinforced concrete buildings. J Earthq Eng 1997;1:157–92.